Applied Ocean Research 74 (2018) 217–226

Contents lists available at ScienceDirect

Applied Ocean Research

journal homepage: www.elsevier.com/locate/apor

Effectiveness of N-waves for predicting morphological changes due to tsunamis

Silvia Chacón-Barrantes

Depto. Fisica, Universidad Nacional, 86-3000 Heredia, Costa Rica, Previously at Coastal Research Laboratory, University of Kiel, Otto-Hahn-Platz 3, D-24098, Kiel, Germany

ARTICLE INFO

Article history:
Received 24 November 2017
Received in revised form 26 January 2018
Accepted 10 March 2018

Keywords:
Tsunami morphological changes
Tsunami sediment transport
Tsunami waveforms
N-waves
Tsunami morphodynamics

ABSTRACT

The research on morphological changes caused by tsunamis has increased considerably in the last few years, yet the processes behind this phenomenon are still not fully understood. This paper analyzes and compares numerical simulations of morphological changes caused by the leading elevation and leading depression N-waves and tsunami waves propagating over a channel with a simple bed slope. The simulations were carried out by means of a coupled flow, sediment transport and morphodynamic two-dimensional-vertical numerical model. The modeled channel bed was composed of cohesionless sediments, and range of values for the bed slope and the wave height were employed. Four tsunami waveforms were studied to test the appropriateness of N-waves in modeling the morphological changes caused by tsunamis. On the modeling performed here, runup values were quite well represented by N-waves. N-waves also represented qualitatively well the morphological changes caused by tsunamis. Yet, values of flow velocities and suspended sediment concentration showed more severe deviations from the modeled results corresponding with tsunami waves, very likely due to differences on the steepness of the waves. Therefore, even when N-waves can and have been used to represent tsunami runup and inundation distance, our results suggest that they should be considered with caution when intended to predict magnitudes of tsunami flow velocities and consequently morphological changes. The use of N-waves to simulate morphological changes caused by tsunamis is not yet converging and must be further investigated.

1. Introduction

Many sediment deposits on the coastal regions around the world have been attributed to sediment transport caused by tsunamis. An active research field has emerged to obtain information about the tsunami that left those deposits behind [1,2]. A large amount of the literature dealing with sediment transport and the resulting morphological changes due to tsunamis is essentially qualitative. For example, many researchers surveyed old sediment deposits to confirm the occurrence of tsunamis [3–5]. In these cases tsunami heights were estimated based on tsunami deposits, as their location is considered an indicator of the minimum possible tsunami inundation limit [6]. However, the extension of inland sediment deposits in proportion to the inundation distance, named the deposition ratio, varies for every tsunami at every location, being in some cases only half of it [7–9].

The sediment transport equations available so far are empirical. These equations have been formulated based on measurements of flow velocities, bed shear stresses and sediment concentrations obtained in rivers under regular circumstances. They are also based on data taken in coastal waters under tides and wind waves. No equations have been formulated specifically for tsunamis. The values measured in coastal waters for wind waves and in rivers are much smaller than those related to tsunamis [10]. Tsunami currents were measured at Hilo Bay, Hawaii during 2011 Japan tsunami [11], and some velocity magnitudes can be estimated from tsunami videos, e.g. Lynett et al. [12]. Nevertheless, there is only one data set on currents and suspended sediment measured during a tsunami and it corresponds to a distant tsunami: the 2010 Chile tsunami arriving to California [13]. The unexpected occurrence of tsunamis makes very difficult to acquire enough datasets of direct measurements of tsunami flow velocities or sediment concentrations for the development of a specific set of equations on tsunami sediment transport. Therefore, the modeling of tsunami morphodynamics is performed employing the only available sediment transport equations even when they might not be completely appropriate.

E-mail address: silvia.chacon.barrantes@una.cr

https://doi.org/10.1016/j.apor.2018.03.006
0141-1187/

Forward numerical modeling of tsunami-driven morphological changes is a relatively new research field. The first approaches were made by Takahashi et al. [14] and Simpson and Castelltort [15]. They presented general sediment transport formulations that can be applied to tsunami modeling. Since then, modeling of morphological changes has been performed mostly with two-dimensional models. In some cases the model was two-dimensional-horizontal or depth-averaged [10,16–21]. In some other cases the model was two-dimensional-vertical, 2DV, considering only one horizontal dimension and variations over the water column [10,22,23]. Some three-dimensional modeling has been performed as well [24–26]. The results achieved so far agreed qualitatively well with measurements of tsunami caused morphological changes, even when in some cases a quantitative agreement was not reached [10,14,22,23]. Those results encourage the use of the currently available sediment transport equations for the computation of morphological changes due to tsunamis. A more extended review of numerical models for tsunami sediment transport, both forward and inverse can be found in Sugawara et al. [2].

One of the recognized models of tsunami sediment transport and morphodynamics is Delft3D [27]. Its flow modulus was validated for simulation of tsunami propagation and runup by Apotsos et al. [23] following the tsunami modeling benchmarks given by Synolakis et al. [28]. Apotsos et al. [10,22,23] extended the model further to simulate tsunami-driven morphological changes along real and modified bathymetric profiles using real tsunami shapes as their input. They established the importance of several factors such as bed roughness, sediment size, composition and distribution on the location and magnitude of the final tsunami driven morphological changes [10,22]. According to their results, the modeling of tsunami morphodynamics requires a larger amount of data than the modeling of the tsunami propagation and inundation solely. Some of these required data are not commonly available, for example parameters that describe the seabed such as the bed roughness coefficient and bed characteristics previous to a tsunami are generally unknown. In the case of bed roughness, the value of the Manning's coefficient depends on some characteristics of the seabed, e.g. the particle size of the sediment, and is rarely uniform. As the value of the Manning's coefficient determines the amount of energy dissipated by friction, it influences the calculated values of flow velocity near the bottom [29] and consequently the erosion and deposition as well. Nevertheless, in tsunami numerical simulations, a uniform value is typically used, as in most cases there is very little information available to consider a heterogeneous distribution of Manning's coefficient. Besides, for the modeling of tsunami morphodynamics it is necessary to have the pre-tsunami bathymetry and topography. The post-tsunami bed levels are also required in the cases of validation and calibration. The limitations on availability of the required data for the modeling of tsunami morphodynamics justify considering other means to gain understanding of the involved processes and obtain general results.

With the same purposes, simplified waveforms are commonly employed in the modeling of tsunami propagation and runup [30]. Tsunami waves can be represented by many simplified waveforms: sinusoidal waves, solitary waves, Cnoidal waves, N-waves, Lorenz waves and Stokes waves (Fig. 1) [31,32], being N-waves and solitary waves the more common representations. For example Apotsos et al. [33] studied the impact on maximum tsunami runup and flow velocity of wave characteristics, bed slope and bottom roughness employing N-waves propagating over a canonical bathymetric profile. N-waves together with solitary waves are employed in the validation of numerical models for tsunami propagation and inundation [28], using only the wave height and equivalent period as the parameters to match tsunami waves.

Some approaches have been made to model tsunami morphodynamics employing simplified waveforms. For example, Cheng and

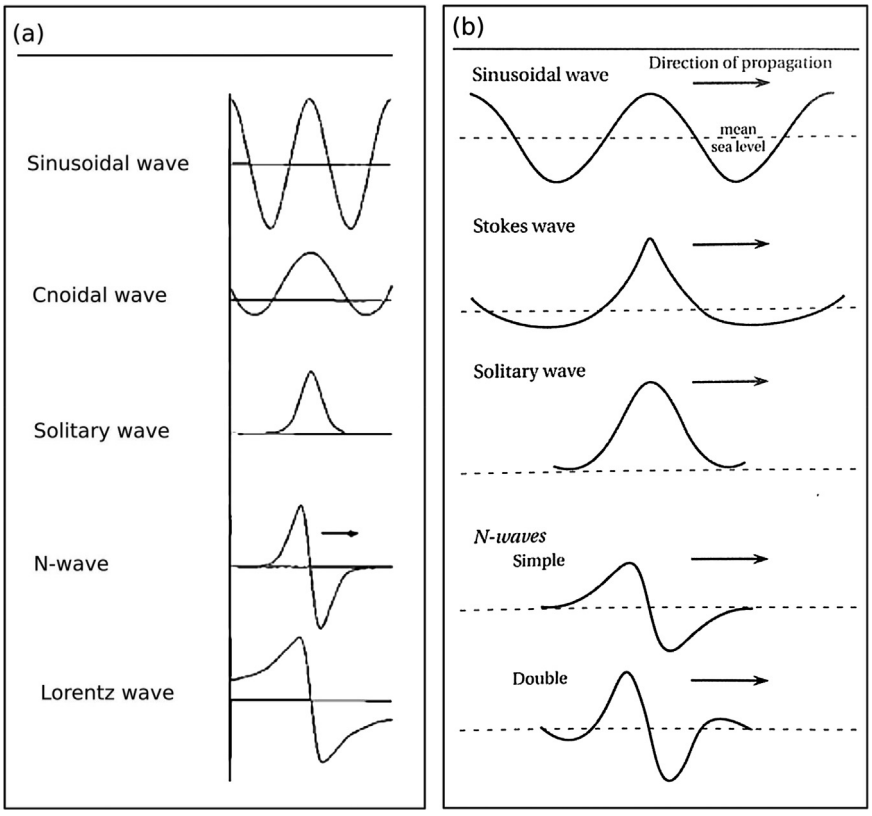

Fig. 1. Simplied waveforms employed to represent tsunami waves. (a) Table 1 from Geist [31]. (b) Fig. 2.4 from Bryant [32].

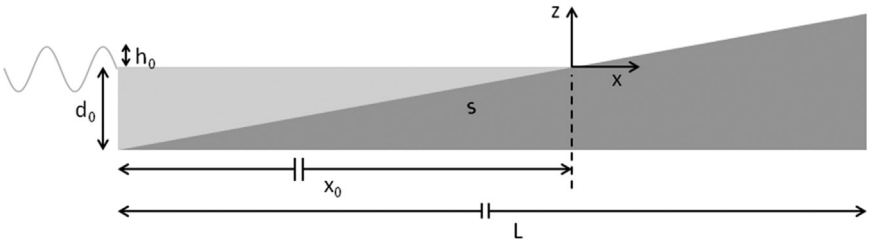

Fig. 2. Schematization of the rectangular channel.

Weiss [34] made a numerical study on the extent of sediment deposition related with the inundation extent using a solitary wave over a canonical bathymetric profile and a simplified sediment deposition model. They found that the deposition ratio depends on the offshore wave amplitude and the onshore slope, and only slightly on the sediment size for sand, at least for this simplified setup. To the knowledge of the author, there are no studies exploring if such results can be extrapolated to real conditions, i.e. real tsunami waveforms or bathymetric profiles.

The aim of this study is to assess if N-waves are suitable to approximate the sediment transport and morphological changes caused by tsunamis. N-waves are considered to represent closely near-shore and far-field tsunamis, based on the bipolarity of the co-seismic deformations [30], whereas the other waveforms have limitations in representing these parameters. N-waves are not expected to reproduce exactly the effects of real tsunami waves, but to approximate them. With this purpose were compared the morphological changes caused by N-waves and tsunami waveforms, including leading elevation (LE) and leading depression (LD) cases. The waves were considered to propagate along a channel with a long constant slope and of which bed was composed of sediments of uniform size. The flow velocity, suspended sediment concentration and morphological changes caused by the waves were analyzed focusing on the uprush and backwash of the waves. Also, were analyzed the morphological changes of equivalent waves with different orientation (leading elevation versus leading depression). The study considered four different tsunami waveforms and their equivalent N-waves. The tsunami waveforms were chosen as it was possible to differentiate their leading wave from their tail. The cases consist on three leading elevation and one leading depression.

2. Methodology

2.1. Numerical model

Here Delft3D modeling system was employed (version 4.00.01). This package was developed at Deltares, Netherlands [35,36], and consists of a 3D coupled flow, sediment transport and morphodynamic model. The flow model solves the non-linear shallow water equations using an alternating directions implicit method [35]. It allows the use of a momentum-advection-explicit scheme for the inundation of dry land [27] which requires Courant numbers less than one for numerical stability. For turbulence, the software employs the k-epsilon model, in which the turbulent kinematic viscosity is related to the turbulent kinetic energy and the energy dissipation rate. The sediment transport formulation used is given by van Rijn [37], differentiating suspended transport and bed load transport for cohesionless sediments. As tsunamis seem to suspend a large amount of sediments, the fluid density is updated at every time step to consider the mass of the suspended sediments. The effect of suspended sediments on fluid stratification is also considered in the model. The bed level is updated at every time step as well.

Delft3D was validated and verified to simulate tsunami propagation and inundation [23]. Currently there are no benchmarks to validate or verify numerical models for the simulation of tsunami morphodynamics. However, several tsunami morphodynamic simulations have been done using Delft3D obtaining encouraging results [22,23,33,38,39].

2.2. Numerical experiment setup

The numerical experiments were performed on a long rectangular channel. The grid consisted on nx cells of 12 m length in the x-direction (cross-shore), one cell of 100 m in the y-direction (alongshore) and 10 σ-layers over the vertical. The thickness of σ-layers decreased from the surface to the bottom in order to achieve better resolution near the bed. Each σ-layer did not have the same thickness or depth over the whole domain, as the number of σ-layers remained constant even though the water depth is not uniform. The results of the numerical model did not vary when the cross-shore grid size was changed to 6 m, hence the x-wise cell length was kept at 12 m. The channel bed had a single slope s and was composed by one class of equally distributed non-cohesive sediments. As sketched in Fig. 2, the horizontal distance x_0 and consequently the number of cells in the x-direction (nx) depended on the bed slope. For all the simulations the maximum water depth was $d_0 = 35$ m and the time step was set to 0.3 s resulting in maximum Courant numbers of about 0.46 at the deepest side of the channel. Delft3D calculates the Courant numbers using the smallest cell size, in this case 12 m.

The bed roughness was characterized by a Manning coefficient of 0.025 $m^{-1/3}$ s, over the entire domain and independent of the sediment size and bed forms. This is the typical value usually adopted for a coast without vegetation [40]. Manning formulation has been employed on the modeling of tsunami morphodynamics in previous studies such as Apotsos et al. [22,23] and Simpson and Castelltort [15]. It is also the standard bed roughness formulation for the numerical simulations of tsunami hydrodynamics [40].

The waves were imposed by means of the so called Riemann boundary condition in order to minimize spurious reflections at the open boundary [41]. Riemann invariant requires knowing the water level and flow velocity of the wave imposed. Apotsos et al. [33] justified the assumption that when imposing N-waves employing the Riemann invariant, it is possible to use the flow velocity derived from shallow water wave theory, $\eta\sqrt{\frac{g}{d}}$ where η is the perturbation of the water level, d is the depth and g is the gravitational acceleration. The same assumption was extended here to the calculation of Riemann invariant for tsunami waves. Apotsos et al. [33] demonstrated that the use of Riemann invariant as a boundary condition eliminates "artificial re-reflections" at the open boundary, making the progressive shallow water wave theory valid over the whole wave signal and the whole domain.

As mentioned before, N-waves were employed as a representation of tsunami waves because of their bipolarity. There are many mathematical formulae to create N-waves; here we employed the

Table 1
Name, orientation, C, and τ of the N-waves employed.

Name and orientation	C (min^{-1})	τ (min)	Matching tsunami wave
A. Leading Elevation	0.14	45	LE Male
B. Leading Elevation	0.12	37	LE Hanimaadhoo
C. Leading Elevation	0.09	50	LE Ganares
D. Leading Depression	0.14	45	LD Male

formulation based on Tadepalli and Synolakis [30] for the simulations:

$$\eta(t)_{x=-x_0} = \mp\frac{3}{2}\sqrt{3}\cdot h_0 sech^2\left[C\left(t-\tau\right)\right] tanh\left[C\left(t-\tau\right)\right], \quad (1)$$

where η is the perturbation of the water level, t is the time, h_0 is the maximum height of the incoming wave, and C and τ are constants determining the width and the central point of the wave respectively. The minus sign in Eq. (1) refers to the leading elevation N-wave (LEN) and the plus sign refers to the leading depression N-wave (LDN). Four N-waves were considered, which constants are listed in Table 1. The parameters of N-waves were chosen to match the period of the corresponding tsunami waveforms, hereafter T-waves (Fig. 3).

Tsunami waveforms were obtained after the recorded 2004 Indonesia tsunami at Ganares, Hanimaadhoo and Male, Maldives [42], and were amplified to a uniform maximum wave height of 4 and 5 m for these simulations (Fig. 3). The leading wave of Male record was similar to N-wave A. This tsunami shape was originally leading elevation and it was inverted to consider also the leading depression case comparing with N-wave D. The leading wave of Ganares and Hanimaadhoo records was similar to N-waves B and C respectively.

Both N-waves and T-waves with initial heights of h_0 = 4 m and 5 m were imposed on the channel with water depth of d_0 = 35 m and bed slope of s = 0.01, 0.015 and 0.02 composed of one class of sediments with medium size between D = 200 μm and 900 μm. However the results presented here correspond to h_0 = 5 m, s = 0.01 and D = 500 μm as the main conclusions of this work did not change when the other values of wave initial height, bed slope and medium sediment size were employed.

3. Results and discussion

3.1. Comparison between N-waves and tsunami waves

3.1.1. Flow velocity and suspended sediment concentration

In this section, we perform a detailed comparison between flow velocity and suspended sediment concentration for N-waves and tsunami waves, by employing case A. Fig. 4 shows the temporal variations along the channel of the superficial horizontal flow velocity and suspended sediment concentration for case A N-wave (top) and T-wave (bottom). Wave development of N-wave after 110 min was not shown because it was zero. The black contours in the plot correspond to zero flow velocity, i.e. flow reversal. The waves were divided in four stages for the analysis:

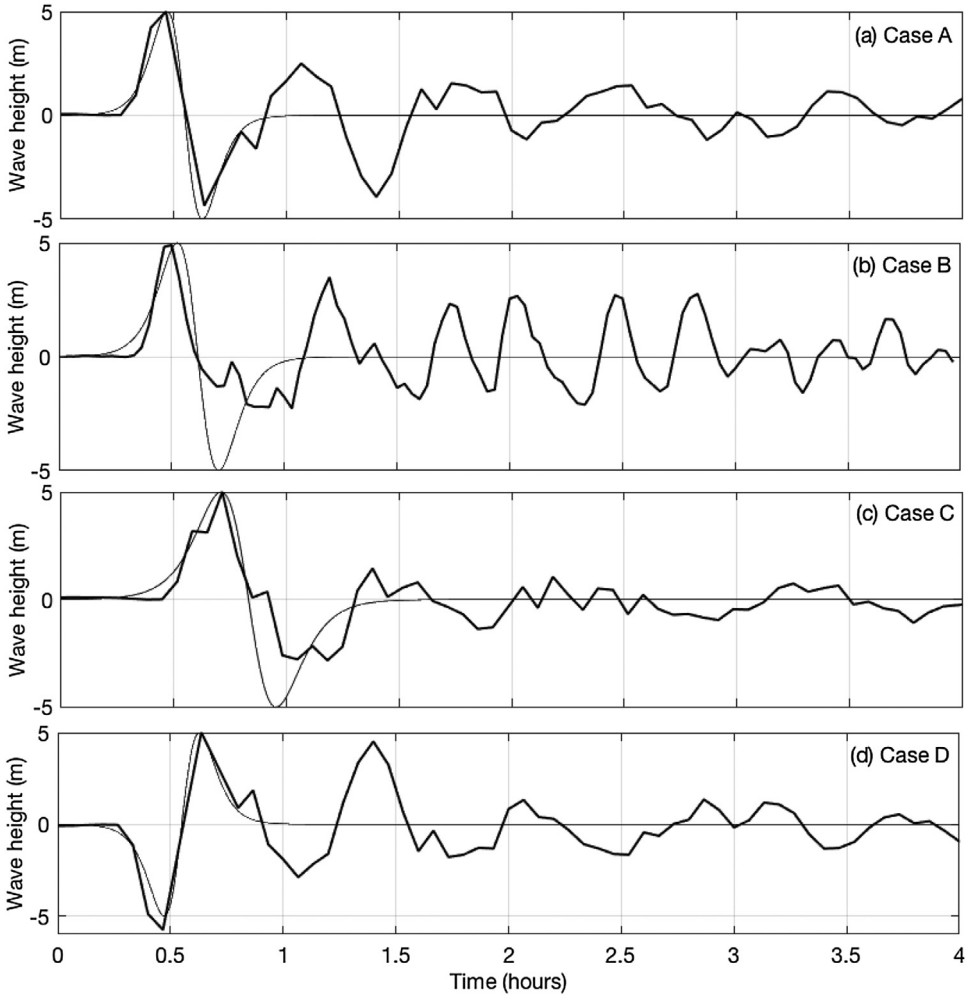

Fig. 3. Waveforms employed in the numerical experiments. Tsunami waveforms are plotted with thick lines and N-waves with thin lines.

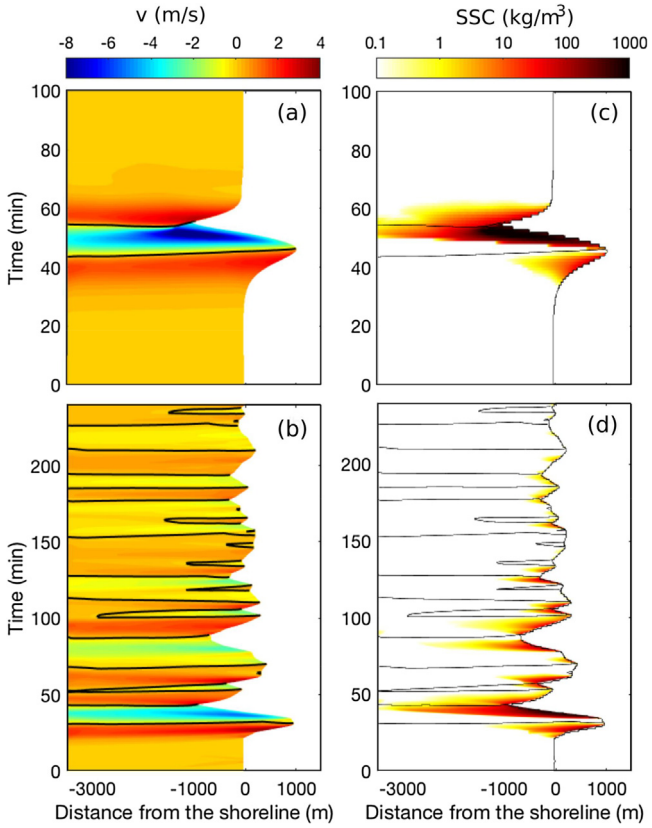

Fig. 4. Superficial flow velocity (m/s) for (a) LEN and (b) leading elevation tsunami waveform. Bottom suspended sediment concentration (SSC) (kg/m^3) for (c) LEN and (d) leading elevation tsunami waveform. Onshore flow velocities are positive and offshore flow velocities are negative. Flow velocity and SSC for LEN after 100 min are not shown, as their values were zero.

1. between the start of movement until first flow reversal: flooding,
2. between the first and second flow reversal: ebbing
3. between the second reversal and zero level again: flooding
4. after the zero level: tsunami-tail, only for T-waves

The maximum superficial flow velocities during the first stage were the smallest for each wave, for case A: 2.54 m/s for the N-wave and 3.65 m/s for the T-wave. The flow velocity was larger for T-waves than for N-waves during this first stage (Fig. 4b darker red vs. Fig. 4a lighter red) as the time derivative $\left(|\frac{\partial \eta}{\partial t}|\right)$ of the former was slightly larger than of the latter (Fig. 5b). During this stage little erosion happened (Fig. 4c and d), due to the relatively small flow velocities.

The second stage had the maximum values of flow velocity magnitude during the whole process, for case A: 8.8 m/s for the N-wave and 5.3 m/s for the T-wave, both corresponding to backwash. Accordingly, the maximum SSC was reached during this stage for both waves (Fig. 4c and d). The flow velocities during this stage were larger for N-waves than for T- waves, as the former had larger $|\frac{\partial \eta}{\partial t}|$ (Fig. 5b). Consequently, N-waves eroded and transported more sediment than T-waves, and this transport was directed offshore in both cases.

During the third stage for N-waves occurred the maximum uprush flow velocity, while the flow returned to its equilibrium level. However, for T- waves the maximum uprush flow velocity occurred during subsequent peaks (fourth stage), and was smaller than for N-waves. Accordingly, there was more sediment suspended during subsequent peaks for the T-waves, than during the third stage.

The high values of sediment concentration obtained were consequence of the high values of flow velocity also modeled (Fig. 4). Both, flow velocity and sediment concentration values were consistent with results of Apotsos et al. [10] who propagated a real tsunami shape on a bed configuration similar to the one employed here. Also, the velocity values obtained here were consistent with results of estimations from real tsunami events. During the 1993 Hokkaido tsunami, the maximum flow velocity was estimated between 10 and 18 m/s at Aonae, Okushiri Island, Japan [43]. During the 2011 Tohoku event at Sendai plain in Japan, the onshore velocity of the wave-front was estimated on about 4 m/s between 1 and 2 km onshore of the original coastline [8]. Lacy et al. [13] were able to measure tsunami currents offshore Monterey Bay, California during the 2010 Chile tsunami. They also measured suspended sediment transport but were not able to separate the transport due to tsunami from the transport due to wind waves. The values they obtained of tsunami currents and suspended sediment transport were much smaller than the values mentioned above and obtained here. However, these measurements referred to a distant tsunami, which are

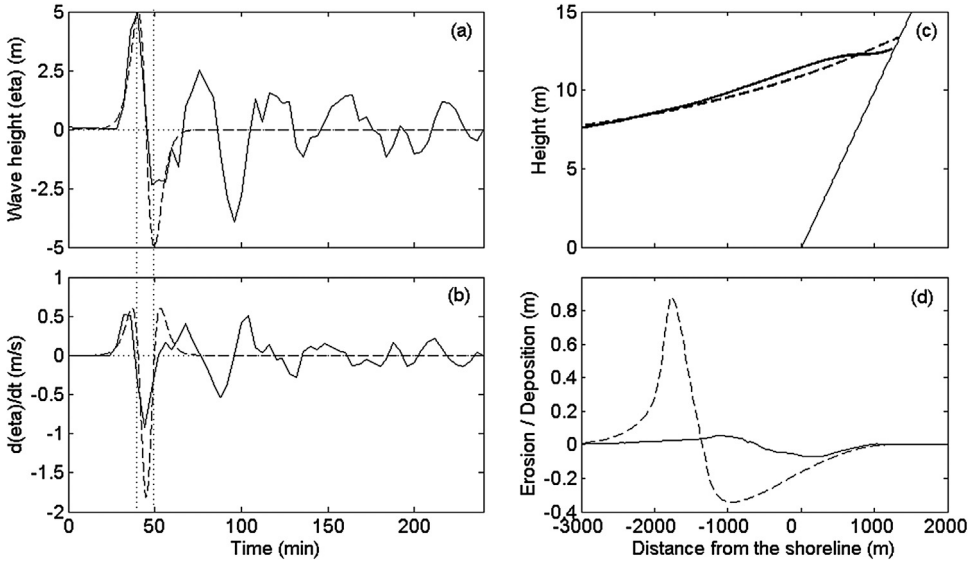

Fig. 5. Case A: (a) Tsunami shape and N-wave. (b) Time derivative of the waves. (c) Maximum water level. (d) Final morphological changes. Lines corresponding to tsunami shapes are solid and to N-waves are dashed. Both cases correspond to s = 0.01 and h_0 = 5 m.

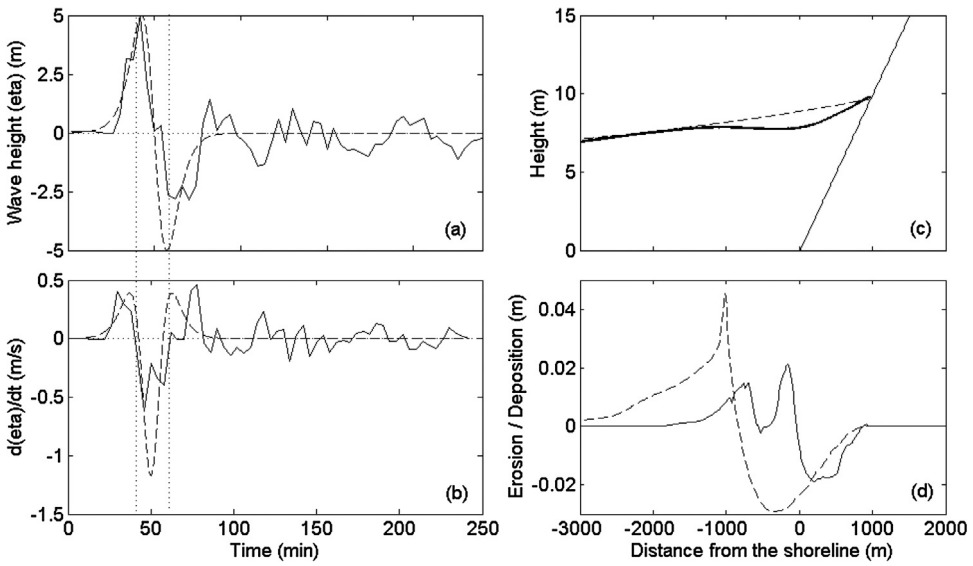

Fig. 6. Case B: (a) Tsunami shape and N-wave. (b) Time derivative of the waves. (c) Maximum water level. (d) Final morphological changes. Lines corresponding to tsunami shapes are solid and to N-waves are dashed. Both cases correspond to s = 0.01 and h_0 = 5 m.

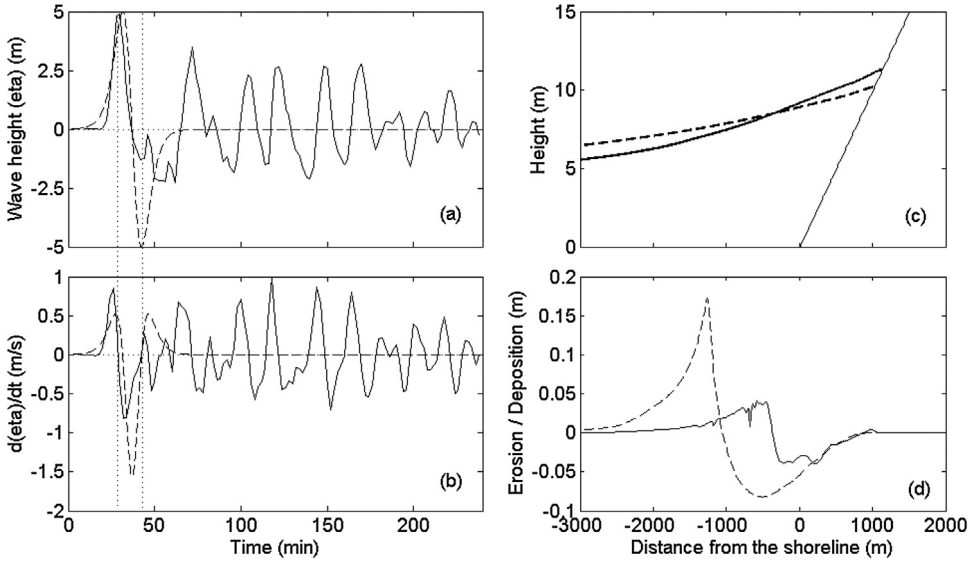

Fig. 7. Case C: (a) Tsunami shape and N-wave. (b) Time derivative of the waves. (c) Maximum water level. (d) Final morphological changes. Lines corresponding to tsunami shapes are solid and to N-waves are dashed. Both cases correspond to s = 0.01 and h_0 = 5 m.

expected to be smaller than those of a local tsunami, and were taken offshore rather than in flooded land. The morphological changes obtained here agreed well with those obtained by Apotsos et al. [22] and also with measurements of real tsunamis, e.g. in Sendai plain after the 2011 Japan tsunami, where the tsunami height was over 10 m, and maximum scour depths of 50 cm together with tsunami deposits as thick as 30 cm were measured [44].

3.1.2. Morphological changes

The magnitude of the morphological changes over the channel bed showed large differences between N-waves and T-waves for all cases (Figs. 5d, 6d, 7d and 8d). For case A and C the final changes had the same shape for both waves, as the T-wave showed only one strong backwash like the LEN (Figs. 5b and 7b, solid lines). This is noticeable on Fig. 4c and d: the largest suspended sediment concentration was located during the first backwash for the LE T-wave, as well as for LEN. Consequently, in these cases the final bed level changes of both T-wave and corresponding N-wave had mainly erosion around the original shoreline and deposition offshore. On case C, the secondary peaks were responsible for the small deposition bump located around x = +1000 m (Fig. 7d), which was not present with the N-wave.

Conversely, the final morphological changes for N-waves and T-waves did not agree qualitatively on case B (Fig. 6d). The small flow reversal around minute 50 on T-wave (Fig. 6a) was responsible of the deposition bump located around x = −100 m (Fig. 6d). The second deposition bump located around x = −700 m resulted when the backwash ceased and the wave started to run up, around minute 70 (Fig. 6a).

For the LD tsunami wave (case D), the presence of several peaks and troughs caused that strong erosion happened during backwash and uprush, unlike LDN for which larger erosion occurred during

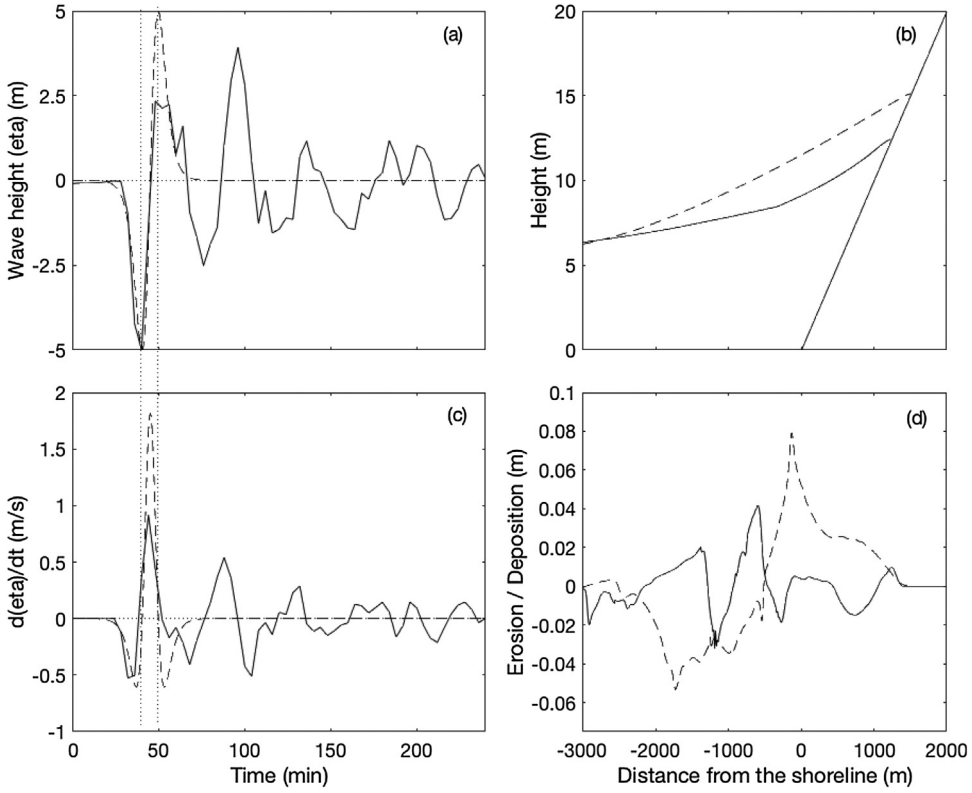

Fig. 8. Case D: (a) Tsunami shape and N-wave. (b) Time derivative of the waves. (c) Maximum water level. (d) Final morphological changes. Lines corresponding to tsunami shapes are solid and to N-waves are dashed. Both cases correspond to s = 0.01 and h_0 = 5 m.

uprush (Fig. 9d and c, respectively). The flow velocity of LD T-wave showed five backwash moments with considerable flow velocity (Fig. 8c solid line) in opposition to LDN where there was only two backwash moments (Fig. 8c dashed line). Consequently, there were four deposition regions for the leading depression T-wave, compared with one for LDN (Fig. 8d).

The tsunami tail of T-waves during the fourth stage performed some rework making the distribution and magnitude of the morphological changes different than for N-waves. However, the main reason for the differences between the magnitude of morphological changes caused by N-waves and T-waves was the steepness of the waveform $|\frac{\partial \eta}{\partial t}|$, leading to large differences in flow velocities and consequently into the sediment eroded and deposited. Even when the leading wave of the tsunami was very similar to N-waves, the T-waves had smaller slopes $\left(|\frac{\partial \eta}{\partial t}|\right)$ than the N-waves during the second stage of the waves. These milder slopes meant that for the T-waves the flow velocities during the second stage were up to almost half than for N-waves. These smaller flow velocities of the T-waves suspended about three times less sediment than N-waves and consequently produced sediment deposits up to ten times thinner than N-waves.

The large quantitative differences between modeled morphological changes caused by T-waves and N-waves showed here were not a result of a particular set of parameters, they were also observed when other values of bed slope were considered, as well as other values of wave height. However, qualitatively there was an agreement on the final morphological changes between T-waves and N-waves for leading elevation cases. Therefore, the author recommends that representation of tsunami-caused morphological changes by N-waves should be done with care and only under qualitative terms.

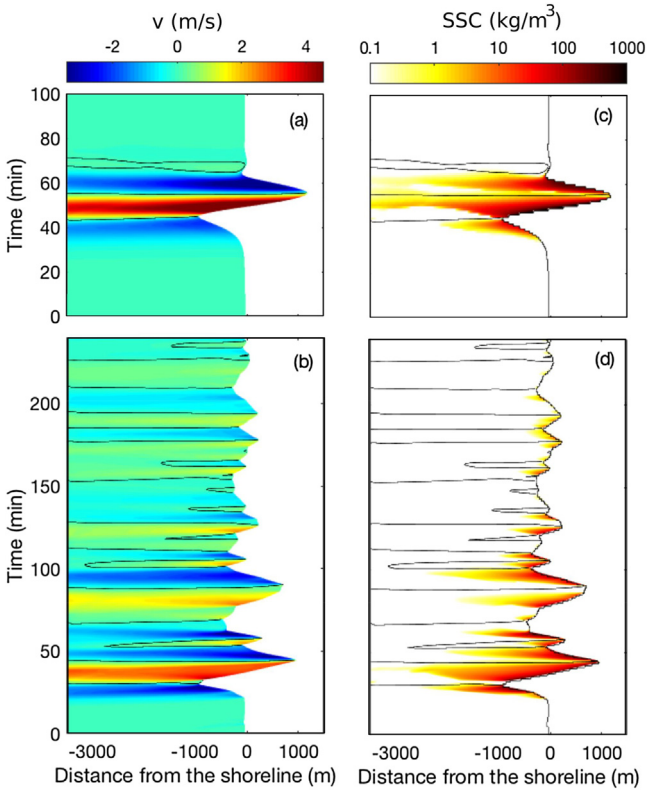

Fig. 9. Superficial flow velocity (m/s) for (a) LDN and (b) leading depression tsunami waveform. Suspended sediment concentration (SSC) (kg/m^3) for (c) LDN and (d) leading depression tsunami waveform. Onshore flow velocities are positive and offshore flow velocities are negative. Flow velocity and SSC for LDN after 100 min are not showed as their values were zero.

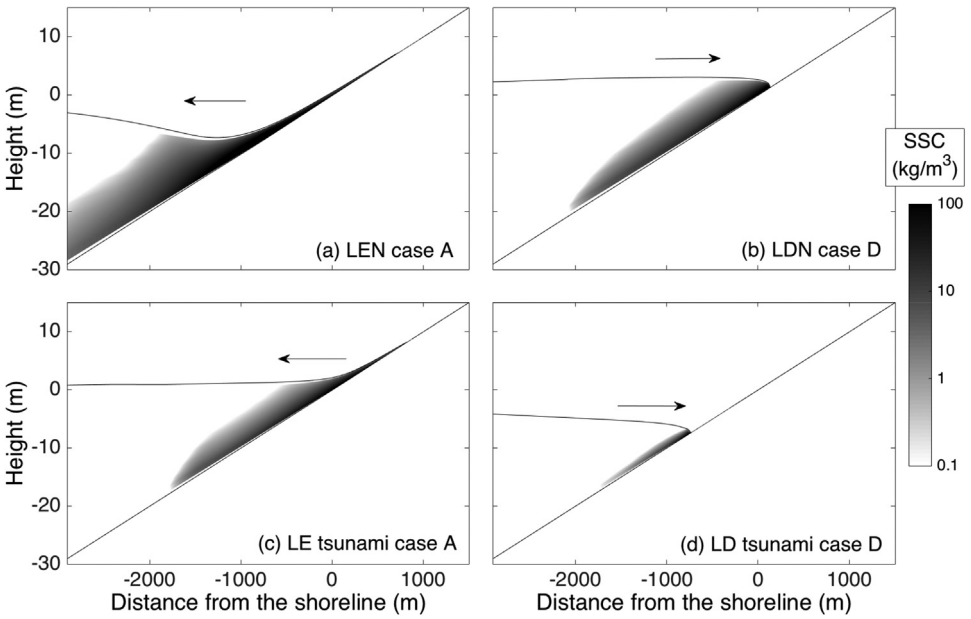

Fig. 10. Suspended sediment concentration (kg/m^3) at the moment of maximum flow velocity for (a) LEN, (b) LDN, (c) LE tsunami waveform and (d) LD tsunami waveform. Arrows indicate flow direction: onshore (positive) and offshore (negative).

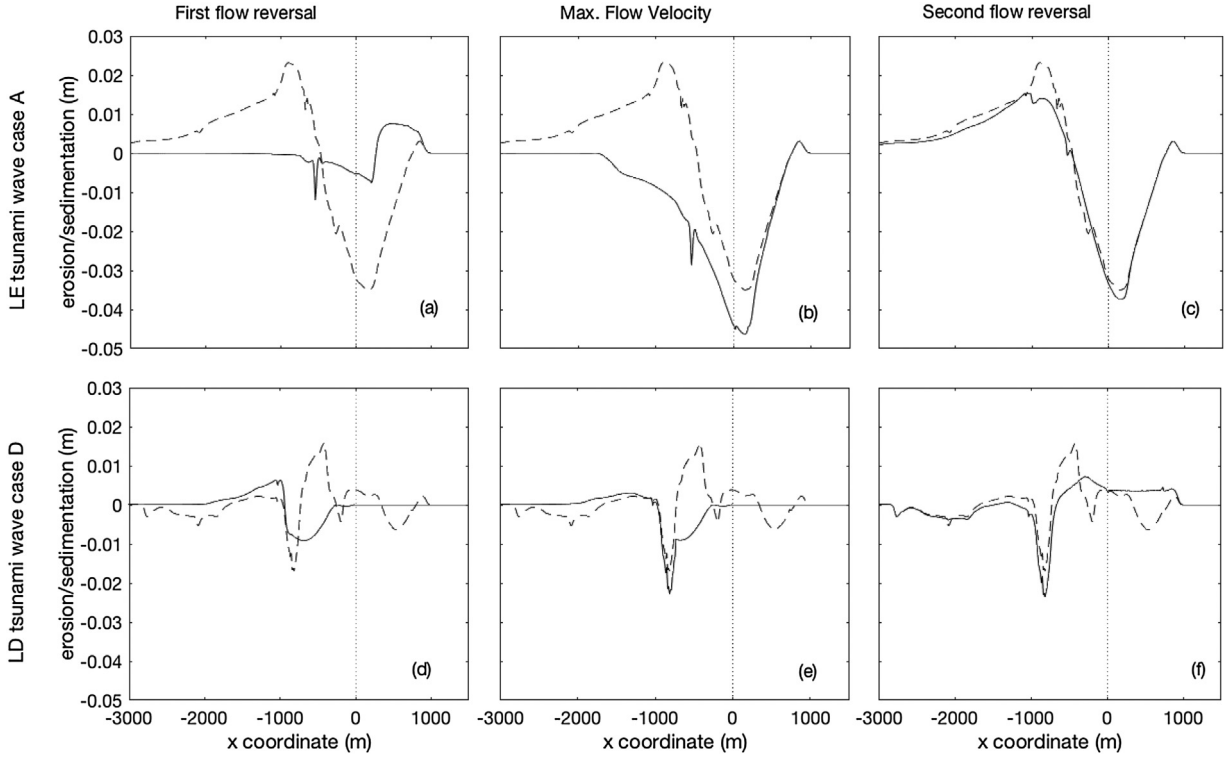

Fig. 11. Instantaneous morphological changes (solid line) for case A LE tsunami wave (top) and case D LD tsunami wave (bottom) at the moments of first flow reversal (left), maximum flow velocity (center) and second flow reversal (right). The final morphological changes are shown with a dashed line in all cases.

3.2. Comparison between leading elevation and leading depression waves

3.2.1. Flow velocities and suspended sediment transport

The flow orientation was opposite for LE and LD waves during the three stages mentioned above. Meaning that the second stage was ebbing for LE and flooding for LD waves, and then the maximum magnitude of flow velocity occurred during backwash flow for LE waves and during uprush flow for LD waves. These results agreed with frictionless results from Carrier et al. [45]. The maximum velocity magnitudes were larger for the LE waves than for the LD waves: 8 m/s vs. 6 m/s corresponding to N-wave cases A and D respectively.

Sediment erosion is extremely sensitive to flow velocities [19]; then, due to the difference on flow velocities, LE cases eroded, suspended (Figs. 4, 9 and 10) and transported more sediment than LD cases during the second stage. This transport was offshore for LE waves and onshore for LD waves. Similar results have been

reported before [46,47] indicating that backwash flows are potentially more erosive than uprush flows, although this was blamed on the channelization caused by coastal topography. This cannot be the reason for the differences obtained here, as we performed two-dimensional-vertical (2DV) numerical simulations and did not considered the along shore direction. The reason for this difference is that in LE waves the gravity, as restoring force, acts on the same direction as the forcing increasing the flow velocity, but for LD it acts in opposite direction as the forcing decreasing the flow velocity.

3.2.2. Morphological changes

During the first flow reversal small deposits formed because small erosion happened through the first stage (Fig. 11 left), which were subsequently eroded during the second stage (Fig. 11 middle). This deposition was located inland for LE waves and offshore for LD waves, thus the final inland deposits for LE were very small compared with offshore deposits. The largest erosion arose during the second stage (Fig. 11 middle and Fig. 10), corresponding with largest flow velocities and largest SSC (Figs. 4 and 9). At the end of this stage, the reversal of the flow allowed larger sediment deposition (Fig. 11 right). This deposition happened mostly around the wave front at that time, offshore for LE waves and around the original coastline and inland for LD waves. Therefore, the orientation of the final bed level changes was opposite for LE waves and LD waves on general terms (Figs. 5d, 6d, 7d and 8d). Those morphological changes were larger for the former than for the later as LE waves suspended more sediment than equivalent LD waves.

This result agreed with Dawson and Stewart [48] who indicated that the oldest tsunami deposits discovered so far were found offshore rather than onshore, and linked this to higher preservation potential in "nearshore low-energy areas" acting like sediment traps. They also pointed that studies on sediment process for recent tsunamis have not included offshore sediment deposits. Those deposits might be an important source of information, due to their higher preservation potential and potentially larger size than onshore deposits, according with our results.

3.3. Vertical distribution of suspended sediment

Although there were moments of very high sediment concentration, most of the suspended sediments were located at the wave front and close to the bottom rather than distributed over the whole water column and the whole channel (Fig. 10). Cheng and Weiss [34] established that "the flow is capable of carrying sand grains in the vicinity of the inundation limit", where the flow depth tends to a limit value. The cause was the relatively small duration of tsunamis and N-waves, which did not allow the suspended sediment to distribute over the whole water column and the whole domain. Nevertheless, for N-wave A the SSC extended further offshore and upper on the water channel than in other cases (Fig. 10a). This would explain the much larger morphological changes caused by this wave with respect to the others. Also, in N-wave D (Fig. 10b) the SSC extended further offshore and upper than for the equivalent T-wave (Fig. 10d), explaining larger erosion and deposition for the former than for the latter. This effect can only be observed employing models considering vertical variations, as the one employed here. Depth-averaged models consider the sediment distributed homogeneously over the water column, leading to non-accurate calculation of sediment erosion and deposition.

4. Conclusions

In this study are presented results of numerical modeling employing Delft3D numerical model. The morphodynamics of leading elevation and leading depression N-waves were described, analyzed and compared with the morphodynamics of equivalent tsunami waveforms, which were normalized to equal maximum wave height.

It was found that even when leading depression waves caused larger runup than leading elevation waves, they caused smaller morphological changes. Furthermore, it was found that the erosion and deposition patterns caused by tsunami waves and N-waves depended on their orientation. For leading elevation cases (both N-waves and tsunami waves) the sediment deposition was located mostly offshore and for LD cases was located inland. The opposite happened with sediment erosion, it was located mostly inland for LE cases and offshore for LD cases. Final morphological changes caused by tsunami waves were composed of several erosion and deposition regions, consequent with the several peaks present in those waves. However, in two of four cases considered here, the magnitude of secondary erosion and deposition regions was very small.

For the cases examined here morphological changes caused by N-waves were much smaller than those caused by tsunami waveforms with equivalent amplitude and period, even when the N-wave caused very similar runup as the correspondent tsunami wave. The large differences on the magnitude of morphological changes were due to the differences on the steepness of the waveform. However, N-waves reproduced qualitatively well the morphological changes caused by tsunami waves on the cases considered here.

Although the numerical modeling of tsunami morphodynamics still has its limitations, its results can be employed to understand better the consequences of tsunamis on a mobile bed. Records of tsunamis that caused morphological changes often consist only of inland sediment deposits and no reference is given to offshore deposits or erosion in general. In the results presented here, leading elevation waves caused both erosion and deposition offshore; therefore, the tsunami surveys should ideally be extended to include determining factors such as the offshore morphological changes.

Acknowledgements

This research was done with an ALECOSTA scholarship from CONARE-Costa Rica and DAAD-Germany. The author wants to thank Dr. Peter Weppen for his valuable comments about the manuscript.

References

[1] B.E. Jaffe, G. Gelfenbaum, A simple model for calculating tsunami flow speed from tsunami deposits, Sediment. Geol. 200 (2007) 347–361, http://dx.doi.org/10.1016/j.sedgeo.2007.01.013.
[2] D. Sugawara, K. Goto, B.E. Jaffe, Numerical models of tsunami sediment transport – current understanding and future directions, Mar. Geol. 352 (2014) 295–320, http://dx.doi.org/10.1016/j.margeo.2014.02.007.
[3] A.G. Dawson, D. Long, D.E. Smith, The Storegga slides: evidence from eastern Scotland for a possible tsunami, Mar. Geol. 82 (1988) 271–276, http://www.sciencedirect.com/science/article/pii/0025322788901466 (Accessed 9 October 2013).
[4] J. Clague, P. Bobrowski, I. Hutchinson, A review of geological records of large tsunamis at Vancouver Island British Columbia, and implications for hazard, Quat. Sci. Rev. 19 (2000) 849–863.
[5] J. Goff, H. Rouse, S. Jones, B. Hayward, U. Cochran, W. McLea, W. Dickinson, M. Morley, Evidence for an earthquake and tsunami about 3100–3400 yr ago, and other catastrophic saltwater inundations recorded in coastal lagoon, Mar. Geol. 170 (2000) 213–249.
[6] A.G. Dawson, The geological significance of tsunamis, Zeitschrift Für Geomorphol. 102 (Suppl. Issues 1) (1996) 199–210.
[7] M.E. Martin, R. Weiss, J. Bourgeois, T.K. Pinegina, H. Houston, V.V. Titov, Combining constraints from tsunami modeling and sedimentology to untanglethe 1969 Ozernoi and 1971 Kamchatskii tsunamis, Geophys. Res. Lett. 35 (2008) L01610, http://dx.doi.org/10.1029/2007GL032349.
[8] K. Goto, J. Takahashi, T. Oie, F. Imamura, Remarkable bathymetric change in the nearshore zone bythe 2004 Indian Ocean tsunami: Kirinda Harbor, Sri Lanka, Geomorphology 127 (2011) 107–116, http://dx.doi.org/10.1016/j.geomorph.2010.12.011.

[9] K. Goto, C. Chagué-Goff, S. Fujino, J. Goff, B.E. Jaffe, Y. Nishimura, B.M. Richmond, D. Sugawara, W. Szczuciński, D.R. Tappin, R.C. Witter, E. Yulianto, New insights of tsunami hazard fromthe 2011 Tohoku-oki event, Mar. Geol. 290 (2011) 46–50, http://dx.doi.org/10.1016/j.margeo.2011.10.004.
[10] A. Apotsos, G. Gelfenbaum, B.E. Jaffe, Process-based modeling of tsunami inundation and sediment transport, J. Geophys. Res. 116 (2011) F01006, http://dx.doi.org/10.1029/2010JF001797.
[11] M.E.M. Arcos, R.J. LeVeque, Validating velocities in the GeoClaw tsunami model using observations near Hawaii fromthe 2011 Tohoku tsunami, Pure Appl. Geophys. 172 (2015) 849–867, http://dx.doi.org/10.1007/s00024-014-0980-y.
[12] P.J. Lynett, J.C. Borrero, R. Weiss, S. Son, D. Greer, W. Renteria, Observations and modeling of tsunami-induced currents in ports and harbors, Earth Planet. Sci. Lett. 327–328 (2012) 68–74, http://dx.doi.org/10.1016/j.epsl.2012.02.002.
[13] J.R. Lacy, D.M. Rubin, D. Buscombe, Currents, drag, and sediment transport induced by a tsunami, J. Geophys. Res. 117 (2012) C09028, http://dx.doi.org/10.1029/2012JC007954.
[14] T. Takahashi, N. Shuto, F. Imamura, D. Asai, Modeling sediment transport due to tsunamis with exchange rate between bed load layer and suspended load layer, Coast. Eng. 2000 – Proc. 27th Int. Conf. (2000) 1508–1519.
[15] G. Simpson, S. Castelltort, Coupled model of surface water flow, sediment transport and morphological evolution, Comput. Geosci. 32 (2006) 1600–1614, http://dx.doi.org/10.1016/j.cageo.2006.02.020.
[16] T. Nishihata, Y. Tajima, Y. Moriya, T. Sekimoto, Topography change due to the Dec 2004 Indian ocean tsunami – field and numerical study at Kirinda Port, Sri Lanka, Coast. Eng. 2006 – Proc. 30st Int. Conf. (2006) 1456–1468.
[17] K. Huntington, J. Bourgeois, G. Gelfenbaum, P.J. Lynett, B.E. Jaffe, H. Yeh, R. Weiss, Sandy signs of a tsunami's onshore depth and speed, Eos Trans. Am. Geophys. Union 88 (2007) 577, http://dx.doi.org/10.1029/2007EO520001.
[18] L. Li, Q. Qiu, Z. Huang, Numerical modeling of the morphological change in Lhok Nga, west Banda Aceh, duringthe 2004 Indian Ocean tsunami: understanding tsunami deposits using a forward modeling method, Nat. Hazards 64 (2012) 1549–1574, http://dx.doi.org/10.1007/s11069-012-0325-z.
[19] B. Ontowirjo, R. Paris, A. Mano, Modeling of coastal erosion and sediment deposition duringthe 2004 Indian Ocean tsunami in Lhok Nga, Sumatra, Indonesia, Nat. Hazards 65 (2012) 1967–1979, http://dx.doi.org/10.1007/s11069-012-0455-3.
[20] W. Szczuciński, M. Kokociński, M. Rzeszewski, C. Chagué-Goff, M. Cachão, K. Goto, D. Sugawara, Sediment sources and sedimentation processesof 2011 Tohoku-oki tsunami deposits on the Sendai Plain, Japan — insights from diatoms, nannoliths and grain size distribution, Sediment. Geol. 282 (2012) 40–56, http://dx.doi.org/10.1016/j.sedgeo.2012.07.019.
[21] D. Sugawara, T. Takahashi, F. Imamura, Sediment transport due tothe 2011 Tohoku-oki tsunami at Sendai: results from numerical modeling, Mar. Geol. 358 (2014) 18–37, http://dx.doi.org/10.1016/j.margeo.2014.05.005.
[22] A. Apotsos, B.E. Jaffe, G. Gelfenbaum, E. Elias, Modeling time-varying tsunami sediment deposition, Coast. Dyn. (2009) 1–15.
[23] A. Apotsos, M. Buckley, G. Gelfenbaum, B.E. Jaffe, D. Vatvani, Nearshore tsunami inundation model validation: toward sediment transport applications, Pure Appl. Geophys. 168 (2011) 2097–2119, http://dx.doi.org/10.1007/s00024-011-0291-5.
[24] T. Nakamura, N. Mizutani, S.C. Yim, A three-dimensional coupled fluid-sediment interaction model with bed-load/suspended-load transport for scour analysis around a fixed structure, J. Offshore Mech. Arrct. Eng. 131 (2009) 31104, http://dx.doi.org/10.1115/1.3124132.
[25] N. Kihara, M. Matsuyama, Numerical simulations of sediment transport induced bythe 2004 Indian ocean tsunami near Kirinda Port in Sri Lanka, Coast. Eng. (2010) 2010.
[26] N. Kihara, N. Fujii, M. Matsuyama, Three-dimensional sediment transport processes on tsunami-induced topography changes in a harbor, Earth Planets Space 64 (2012) 787–797, http://dx.doi.org/10.5047/eps.2011.05.036.
[27] G.S. Stelling, S.P.A. Duinmeijer, A staggered conservative scheme for every Froude number in rapidly varied shallow water ows, Int. J. Numer. Methods Fluids 43 (2003) 1329–1354, http://dx.doi.org/10.1002/?d.537.
[28] C.E. Synolakis, E.N. Bernard, V.V. Titov, U. Kânoğlu, F.I. González, Validation and verification of tsunami numerical models, Pure Appl. Geophys. 165 (2008) 2197–2228, http://dx.doi.org/10.1007/s00024-004-0427-y.
[29] G. Gayer, S. Leschka, I. Nöhren, O. Larsen, H. Günther, Tsunami inundation modelling based on detailed roughness maps of densely populated areas, Nat. Hazards Earth Syst. Sci. 10 (2010) 1679–1687, http://dx.doi.org/10.5194/nhess-10-1679-2010.
[30] S. Tadepalli, C.E. Synolakis, Model for the leading waves of tsunamis, Phys. Rev. Lett. 77 (1996) 2141–2145.
[31] E.L. Geist, Local tsunamis and earthquake source parameters, Adv. Geophys. 39 (1997) 117–209, http://dx.doi.org/10.1016/S0065-2687(08)60276-9.
[32] E. Bryant, Tsunami The Underrated Hazard, 1 st ed., Springer, Chichester, UK, 2008.
[33] A. Apotsos, B.E. Jaffe, G. Gelfenbaum, Wave characteristic and morphologic effects on the onshore hydrodynamic response of tsunamis, Coast. Eng. 58 (2011) 1034–1048, http://dx.doi.org/10.1016/j.coastaleng.2011.06.002.
[34] W. Cheng, R. Weiss, On sediment extent and runup of tsunami waves, Earth Planet. Sci. Lett. 362 (2013) 305–309, http://dx.doi.org/10.1016/j.epsl.2012.12.004 (Accessed 5 August 2013).
[35] J.J. Leendertse, A Three-Dimensional Alternating Direction Implicit Model with Iterative Fourth-Order Dissipative Non-Linear Advection Terms, 1987.
[36] G.R. Lesser, J.a. Roelvink, J.a.T.M. van Kester, G.S. Stelling, Development and validation of a three-dimensional morphological model, Coast. Eng. 51 (2004) 883–915, http://dx.doi.org/10.1016/j.coastaleng.2004.07.014.
[37] L.C. van Rijn, Principles of Sediment Transport in Rivers, Estuaries and Coastal Seas, 1993.
[38] A. Apotsos, G. Gelfenbaum, B.E. Jaffe, Process-based modeling of tsunami inundation and sediment transport, J. Geophys. Res. 116 (2011) F001797, http://dx.doi.org/10.1029/2010JF001797.
[39] A. Apotsos, G. Gelfenbaum, B.E. Jaffe, S. Watt, B. Peck, M. Buckley, A. Stevens, Tsunami inundation and sediment transport in a sediment-limited embayment on American Samoa, Earth-Sci. Rev. 107 (2011) 1–11, http://dx.doi.org/10.1016/j.earscirev.2010.11.001.
[40] B. Levin, M.A. Nosov, Physics of Tsunamis, Springer, 2009.
[41] G.K. Verboom, A. Slob, Weakly-reactive boundary conditions for two-dimensional water flow problems, Adv. Water Resour. 7 (1984) 192–197.
[42] UHSLC, University of Hawaii Sea Level Center, 2013 http://ilikai.soest.hawaii.edu/uhslc/.
[43] A. Tsutsumi, T. Shimamoto, E. Kawamoto, J. Logan, Nearshore flow velocity of Southwest Hokkaido earthquake tsunami, J. Waterw. Port Coast. Ocean Eng. 126 (2000) 136–143, http://dx.doi.org/10.1061/(ASCE)0733-950X(2000)126:3(136).
[44] B.M. Richmond, W. Szczuciński, C. Chagué-Goff, K. Goto, D. Sugawara, R.C. Witter, D.R. Tappin, B.E. Jaffe, S. Fujino, Y. Nishimura, J. Goff, Erosion, deposition and landscape change on the Sendai coastal plain, Japan, resulting fromthe March 11, 2011 Tohoku-oki tsunami, Sediment. Geol. 282 (2012) 27–39, http://dx.doi.org/10.1016/j.sedgeo.2012.08.005.
[45] G.F. Carrier, T.T. Wu, H. Yeh, Tsunami run-up and draw-down on a plane beach, J. Fluid Mech. 475 (2003), http://dx.doi.org/10.1017/S0022112002002653.
[46] G. Einsele, S.K. Chough, T. Shiki, Depositional events and their records – an introduction, Sediment. Geol. 104 (1996) 1–9.
[47] J.P. Le Roux, G. Vargas, Hydraulic behavior of tsunami backflows: insights from their modern and ancient deposits, Environ. Geol. 49 (2005) 65–75, http://dx.doi.org/10.1007/s00254-005-0059-2.
[48] A.G. Dawson, I. Stewart, Tsunami deposits in the geological record, Sediment. Geol. 200 (2007) 166–183, http://dx.doi.org/10.1016/j.sedgeo.2007.01.002.